SCIENTIFIC REPORTS

OPEN

SUBJECT AREAS:
APPLIED OPTICS
OPTICAL TECHNIQUES

Received
14 August 2014

Accepted
21 November 2014

Published
11 December 2014

Correspondence and requests for materials should be addressed to J.W. (jwang@hust.edu.cn)

Arbitrary manipulation of spatial amplitude and phase using phase-only spatial light modulators

Long Zhu & Jian Wang

Wuhan National Laboratory for Optoelectronics, School of Optical and Electronic Information, Huazhong University of Science and Technology, Wuhan 430074, Hubei, China.

Spatial structure of a light beam is an important degree of freedom to be extensively explored. By designing simple configurations with phase-only spatial light modulators (SLMs), we show the ability to arbitrarily manipulate the spatial full field information (i.e. amplitude and phase) of a light beam. Using this approach to facilitating arbitrary and independent control of spatial amplitude and phase, one can flexibly generate different special kinds of light beams for different specific applications. Multiple collinear orbital angular momentum (OAM) beams, Laguerre-Gaussian (LG) beams, and Bessel beams, having both spatial amplitude and phase distributions, are successfully generated in the experiments. Some arbitrary beams with odd-shaped intensity are also generated in the experiments.

Spatial light modulators (SLMs) are widely used as diffractive optical elements (DOEs) in optical systems to facilitate flexible control of light beams. In diffractive techniques, specific pattern is written onto the SLM by a computer, and the input spatial light is modulated by the relevant pattern. Thus, it is a simple and convenient approach to control the spatial light by using the SLMs. Novel applications of SLMs in different areas have been proposed, such as diffractive optics[1], optical metrology[2], programmable adaptive optics[3], laser pulse shaping[4], real world 3-D holographic projection systems[5], optical tweezers[6], optical information processing[7], polarization control[8,9], vector beams generation[10,11] and orbital angular momentum (OAM) communications[12–14].

OAM beam is a helically phased beam comprising an azimuthal phase term $\exp(il\varphi)$, possessing an OAM of $l\hbar$ per photon, where l is referred to topological charge and φ is the azimuthal angle[15–17]. In 2004, G. Gibson et al. experimentally demonstrated the transfer of information encoded as OAM states of a light beam by loading the computer-controlled phase hologram onto the SLM[18]. Recently, in OAM based optical communication systems, phase-only SLMs are widely used as the key devices for generating different states of OAM beams to increase the communication capacity and spectral efficiency[12–14].

Remarkably, most of the SLMs employed in the experiments are phase-only elements, which are mainly used to shape the spatial phase distribution of the light beam directly without touching the amplitude distribution. So it is not straightforward to fully control the light beam by a single phase-only SLM in general. However, full field (i.e. amplitude and phase) control is always highly desirable in order to generate different types of light beams with special properties. In this scenario, a laudable goal would be to develop novel schemes or configurations to arbitrarily manipulate both the spatial amplitude and phase of the incoming light beam. So far, some previous works dealing with the manipulation of phase and amplitude have been reported with impressive performance[19–25]. One technique is to make use of a modified hologram by modulating the phase height of the grating programmed into the hologram[19–22]. Actually, the amplitude at any point in a plane can be controlled by adjusting the efficiency of the blazing in the corresponding region of the hologram. One can simply impose the desired intensity of the beam with some modifications to account for the mapping of phase height to diffraction efficiency to produce the hologram. The other technique is based upon two cascaded holograms, arranged in an optical 2-f setup, where the first hologram is designed to create the desired amplitude in the plane of the second hologram which further imprints the desired phase[23–25]. A couple of so-called phase retrieval algorithms, such as Gerchberg-Saxton algorithm[26], can be utilized to introduce the desired amplitude modulation as exactly as possible in the Fourier plane of the first hologram (i.e. plane of the second hologram). The amplitude modulation is achieved by shaping only the phase with the first hologram, relying on propagation and interference to form the amplitude.

In this paper, we propose an alternative simple method to arbitrarily manipulate the amplitude and phase of the incoming light beam with two phase-only SLMs without using any phase iterative algorithm. By using this

method, we show the successful generation of multiple collinear OAM beams, Laguerre-Gaussian (LG) beams, Bessel beams, and some arbitrary beams with odd-shaped intensity in the experiments.

Results

Concept and principle. The concept and principle of arbitrary manipulation of amplitude and phase of a light beam with two cascaded SLMs is illustrated in Fig. 1. We set the polarization direction of the input light A_0 45° with respect to the x direction. The working direction of polarization-dependent SLM1 is x direction with a phase distribution $\varphi_1(x, y)$. After the SLM1, the light is half modulated, with the x direction distribution $\frac{\sqrt{2}}{2}A_0 \cdot \exp(i\varphi_1(x,y))$ and y direction distribution $\frac{\sqrt{2}}{2}A_0$. And then, the light beam passes through a polarizer with the polarization direction 45° deviation from the x direction. Thus, the electrical field of light beam becomes

$$E(x,y) = \frac{\sqrt{2}}{2}A_0(\exp(i\varphi_1(x,y)) \times \frac{\sqrt{2}}{2} + \frac{\sqrt{2}}{2}A_0 \times \frac{\sqrt{2}}{2} = \frac{1}{2}A_0(\exp(i\varphi_1(x,y)) + 1) \quad (1)$$

After the polarizer, the light comes through the SLM2 with a phase distribution $\varphi_2(x, y)$. The working direction of polarization-dependent SLM2 keeps the same as the light polarization after the polarizer, which is actually enabled by adjusting the light polarization after the polarizer via a half-wave plate placed between the polarizer and SLM2. So the electrical field of light after the SLM2 becomes

$$E(x,y) = \frac{1}{2}A_0(\exp(i\varphi_1(x,y)) + 1)\exp(i\varphi_2(x,y)) = A_0\cos(\frac{\varphi_1(x,y)}{2})\exp(i\frac{\varphi_1(x,y) + 2\varphi_2(x,y)}{2}) \quad (2)$$

From Eq. (2), one can easily find that the amplitude distribution is determined by $\varphi_1(x, y)$, and the phase distribution is determined by $\frac{1}{2}\varphi_1(x,y) + \varphi_2(x,y)$. So, by changing the phase distribution patterns written onto the SLM1 and SLM2, we can manipulate the amplitude and phase independently at the same time. By using this method, we can arbitrarily generate different types of light beams as desired, such as multiple collinear OAM beams, LG beams, Bessel beams and so on.

Experimental setup. The key elements in the experimental setup are two phase-only SLMs. Considering the fact that the phase and amplitude might change upon propagation between the two SLMs, we add lenses between the two SLMs and develop two imaging systems with unit magnification, as shown in Fig. 2. The added lenses in the imaging systems facilitate the cancellation of spurious phase delays caused by the propagation between two SLMs.

As shown in Fig. 2(a), System A is a one-lens imaging system. The distance between the two SLMs is 600 mm. The focal length f of the lens is 150 mm. The one-lens imaging system images the plane of SLM1 to that of SLM2 with unit magnification. The one-lens imaging system (System A) can retrieve both amplitude and phase information of SLM1 plane at the position of SLM2 plane, although an additional radial phase distribution $\exp\left(i\frac{k}{2f}(x^2+y^2)\right)$ is introduced.

As shown in Fig. 2(b), System B is a well-known 4f system with two lenses placed between the two SLMs at equal spacing of focus length f. The distance between the two SLMs is also 600 mm and the focal length f of the two lenses is 150 mm. The 4f system also images the plane of SLM 1 to that of SLM 2 with unit magnification. In particular, no additional radial phase distribution as in System A is introduced in System B, i.e. almost perfect imaging from the SLM1 plane to the SLM2 plane is obtained.

In both System A and System B, the light comes from a laser with a wavelength of 1550 nm, and collimated by a collimator. The collimated light beam passes through the polarizer (Pol1) and half-wave plate (HWP1). The Pol1 and HWP1 are used to change the polarization of the input light 45° deviation from the working direction of the SLM1, which makes the input light partly modulated. And then, we adjust Pol2 to align its polarization direction 45° with respect to the working direction of the SLM1 and rotate HWP2 to make the polarization of the light in agreement with the working direction of the SLM2. The imaging systems (System A, System B) image the plane of SLM1 to that of SLM2, removing the unwanted phase distribution due to propagation from SLM1 to SLM2. As a consequence, the amplitude and phase of the light are modulated by the two phase patterns written onto the SLMs. At last, we use a camera to capture the intensity distribution of the output light beam.

Generation of multiple collinear OAM beams. We first demonstrate the generation of multiple collinear OAM beams. The experimental results are shown in Fig. 3. We generate three groups

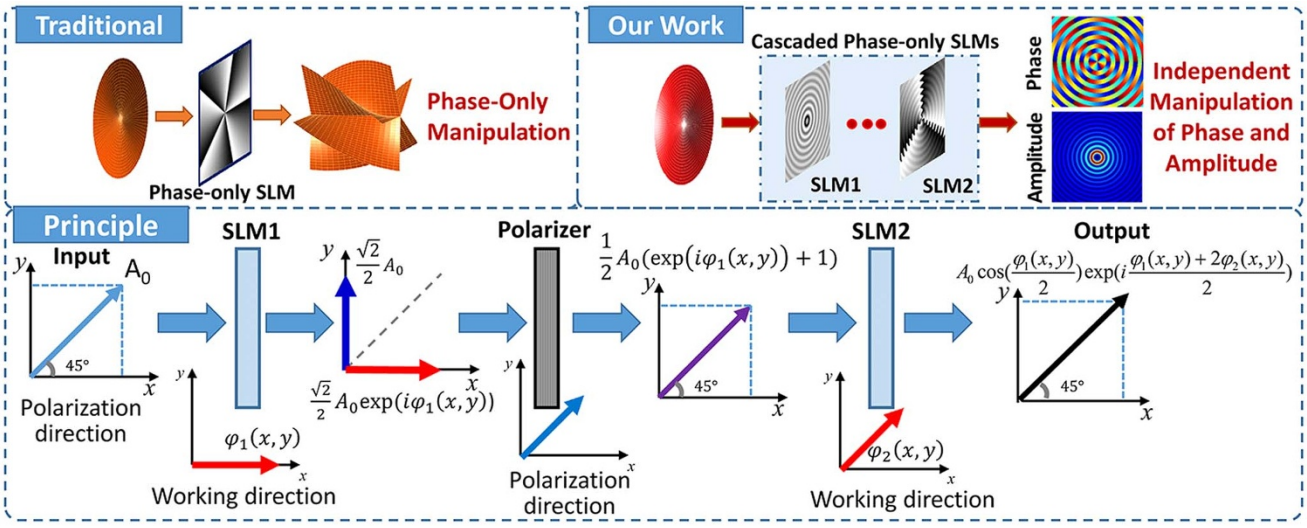

Figure 1 | Concept and principle of arbitrary full-field (i.e. amplitude and phase) manipulation of a light beam with two phase-only SLMs.

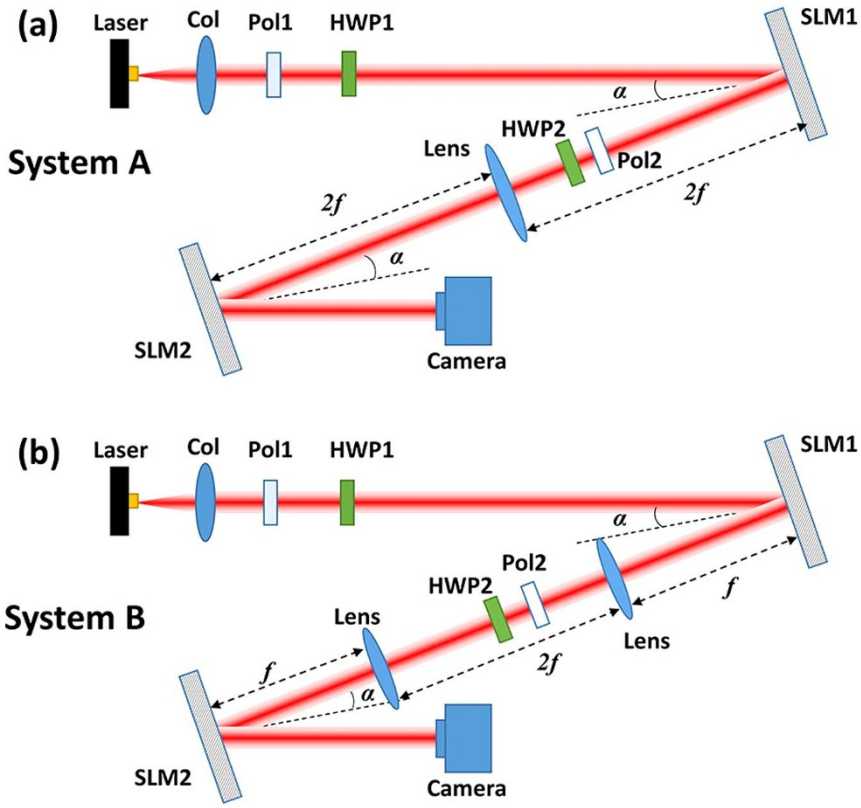

Figure 2 | **Experimental setup.** (a) One-lens imaging system (System A). (b) 4f system (System B). Col: collimator, Pol: polarizer, HWP: half-wave plate, SLM: spatial light modulator.

of multiple collinear OAM beams, $OAM_{+3,+6,+9,+12}$ (i.e. superimposed multiple collinear OAM beams containing OAM modes with topological charges of $l = +3$, $+6$, $+9$ and $+12$), $OAM_{+5,+10,+15,+20}$ and $OAM_{+3,+9,+15,+21}$. The intensity profiles of the generated multiple collinear OAM beams are shown in Fig. 3(a). The first line is the theoretical results for comparison. The second line shows the measured intensity profiles after the amplitude and phase modulations of two SLMs by the imaging System A, and the third line shows the measured intensity profiles by the imaging System B. One can see that both of the two imaging systems generate multiple collinear OAM beams with dark spot appearing at the center of the intensity profiles. The obtained experimental results are in agreement with the theory as expected. Shown in Fig. 3(b) are typical two phase patterns loaded onto SLM1 and SLM2 to generate three collinear OAM beams of $OAM_{+5,+10,+15,+20}$.

In order to identify the states of the generated multiple collinear OAM beams, we use another SLM loading a series of spiral phase patterns (e.g. from $l = -1$ to $l = -25$) to demodulate each OAM state, respectively. When one of the generated OAM beams (e.g. $l = +5$) meets its inverted spiral phase pattern (e.g. $l = -5$), the helical phase front of the OAM beam will be removed, resulting in the demodulation from an OAM beam to a Gaussian-like beam with a planar phase front. In contrast, another spiral phase pattern (e.g. $l = -2$), used to demodulate none generated OAM beam (e.g. $l = +2$), only changes the topological charge of the generated OAM beam (e.g. from $l = +5$ to $l = +3$) which still has a helical phase front. Owing to the central phase singularity of helical phase front, OAM beam features a doughnut shape intensity profile with no intensity at the center, while the demodulated Gaussian-like beam (planar phase front) from a particular OAM beam has a central bright high-intensity spot. Consequently, it is possible to determine a particular OAM beam from its demodulated Gaussian-like beam (bright central spot) by employing a specific spiral phase pattern with an inverted topological charge. In Fig. 4, we show the demodulated intensity profiles of $OAM_{+5,+10,+15,+20}$ for the two imaging systems. We find that the demodulated intensity profiles for $l = +5$, $+10$, $+15$ and $+20$ have bright spots at the center as shown in the first line. Other demodulated intensity profiles using spiral phase patterns for none generated OAM states ($l = +2$, $+7$, $+12$ and $+17$) have no intensity at the center, which are shown in the second line.

Generation of LG beams. We then generate a series of pure LG beams and their superposition by the two phase-only SLMs. LG beams are the most common beams carrying OAM, which also have amplitude distributions. In an LG_{pl} beam, l is the azimuthal index giving an OAM distribution, and p is the number of radial nodes in the intensity distribution. By calculating the theoretical electrical field of target LG beam, we can get the amplitude and phase distribution. Through Eq. (2), we can calculate the corresponding phase patterns $\varphi_1(x, y)$ and $\varphi_2(x, y)$, which are loaded onto the two SLMs. The theoretical and experimental results for the two imaging systems are shown in Fig. 5(a). We also generate the superposition of LG_{05} and $LG_{0\text{-}5}$. It can be seen that there are ten bright spots in the experimental results in both of the two imaging systems, which are in agreement with theory. The obtained results shown in Fig. 5(a) indicate the feasibility of arbitrary manipulation of amplitude and phase using the proposed approaches. Shown in Fig. 5(b) are the phase patterns loaded onto SLM1 and SLM2 for generating the superposition of LG_{05} and $LG_{0\text{-}5}$.

Generation of Bessel beams. By using the two phase-only SLMs, we then generate Bessel beams by the two imaging systems. Bessel beam is normally known as the non-diffraction beam, which propagates in free space without any spreading. Zero-order Bessel beam has a central bright spot, whereas high-order Bessel beams have a central dark region. In particular, higher-order Bessel beams are OAM-carriers. These higher-order Bessel beams propagate and maintain

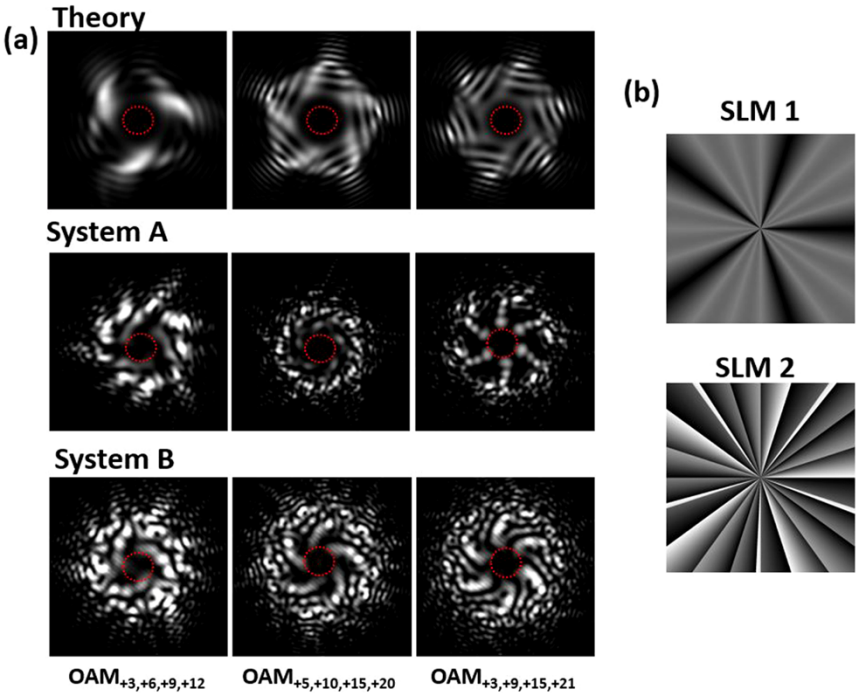

Figure 3 | Theoretical and experimental results for the generation of multiple collinear OAM beams. (a) Intensity profiles of the generated multiple collinear OAM beams ($OAM_{+3,+6,+9,+12}$, $OAM_{+5,+10,+15,+20}$ and $OAM_{+3,+9,+15,+21}$). (b) Phase patterns loaded onto SLM1 and SLM2 for generating $OAM_{+5,+10,+15,+20}$.

their cross-sectional form over a finite distance[27–29]. Moreover, they can reconstruct after encountering an obstacle[30–32]. Exploiting these properties of Bessel beams may make them useful in the field of long-range free-space communication systems.

We calculate the desired phase patterns for generating three Bessel beams, $l = 0$, $+1$ and $+3$. The experimental results are shown in Fig. 6. The first line of Fig. 6(a) is the theoretical results. The second and third lines of Fig. 6(a) are the measured intensity profiles of the generated Bessel beams.One can see that the center of the zero-order Bessel beam ($l = 0$) exists a bright spot, whereas high-order Bessel beams ($l = +1, +3$) have a central dark region. We can also find that the central dark region of the high-order Bessel beam becomes larger with the increase of the topological charge, which is consistent with the theory. In order to identify the phase distribution of the generated Bessel beams, we measure the interferograms, i.e. the interference between generated Bessel beams and a Gaussian beam reference. Because of the phase singularity, a dislocated interference fringe is observed when a Bessel beam and a Gaussian beam interfere with a small angle. The obtained results are shown in Fig. 6(b). One can clearly see that the experimental results are in good agreement with theoretical ones. Fig. 6(c) shows the phase patterns loaded onto SLM1 and SLM2 for generating the Bessel beam with $l = +3$.

Generation of arbitrary beams with odd-shaped intensity. Finally, in order to show the arbitrary manipulation of spatial amplitude, we employ two phase-only SLMs to generate arbitrary beams with odd-shaped intensity using the 4f system (System B). The experimental results are shown in Fig. 7. The first line of Fig. 7 is the desired odd-shaped intensity of different light beams. The second and third lines of Fig. 7 are the designed phase patterns loaded onto SLM1 and SLM2, respectively. The observed experimental results are shown in the last line. It can be clearly seen that the experimental results are almost the same as the desired ones. The obtained results indicate that one can arbitrarily manipulate the spatial amplitude of incident light beams using the proposed approaches.

Discussion

In conclusion, we present a simple and efficient method for arbitrarily manipulating the amplitude and phase of a light beam independently with two phase-only SLMs. We demonstrate the successful

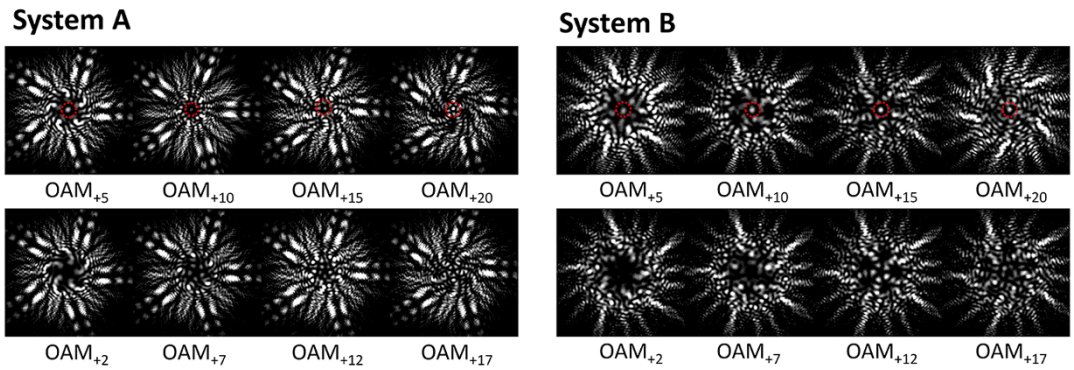

Figure 4 | Measured demodulated intensity profiles of $OAM_{+5,+10,+15,+20}$ by the two imaging systems (System A, System B).

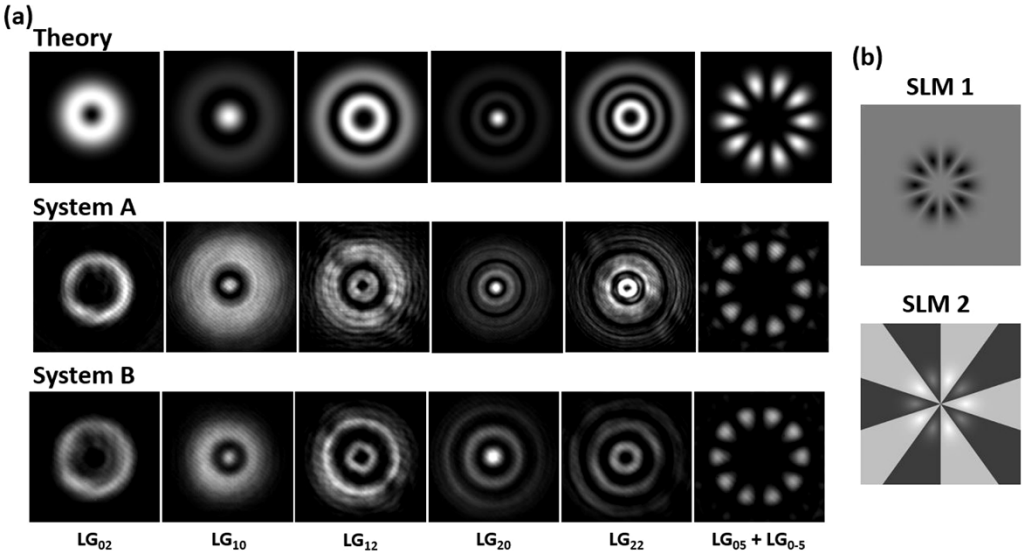

Figure 5 | (a) Theoretical and experimental results for the generation of LG beams and their superposition (LG_{02}, LG_{10}, LG_{12}, LG_{20}, LG_{22}, LG_{05} + $LG_{0\text{-}5}$) by the two imaging systems. (b) Phase patterns loaded onto SLM1 and SLM2 for generating the superposition of LG_{05} and $LG_{0\text{-}5}$.

generation of multiple collinear OAM beams, LG beams and Bessel beams in the experiments. We also compare the experimental results with the theory. By using this method, it might be possible to arbitrarily generate different special light beams for specific applications. This flexible approach to enabling arbitrary full-field (i.e. amplitude and phase) control of light beams may open a door to facilitate more applications in free-space optical communications.

Remarkably, we use two SLMs to perform the manipulation of amplitude and phase. For the original idea, the second SLM should be placed right after the first SLM, i.e. no distance between the two SLMs, which is however impossible in practical operations as additional polarizer and half-wave plate need to be placed between the two SLMs. So it is unavoidable to separate the two SLMs with a distance which might cause unwanted phase distributions. Hence, it is critical to remove the influence from the spurious phase delays upon propagation between the two SLMs, which could be enabled by lenses in well-established imaging systems. Such phenomena can be explained and theoretically analyzed as follows for the two employed imaging systems (System A, System B) based on Fourier optics (scalar diffraction theory, Fresnel diffraction integral, phase transformation of lens)[33].

For the one-lens imaging system (System A), as illustrated in Fig. 8(a), we assume the input light from SLM1 to be $A(\zeta, \eta)$. Coming out of the SLM1, the light passes through the lens f, and is focused by the lens. We can get the light distribution $U_f(u, v)$ at the lens focus plane expressed by

$$U_f(u,v) = \frac{\exp\left[-j\frac{k}{2f}(u^2+v^2)\right]}{j\lambda f} \times \iint A(\xi,\eta)\exp\left[-j\frac{2\pi}{\lambda f}(\xi u+\eta v)\right]d\xi d\eta \quad (3)$$

After that, the light propagates distance f and arrives at SLM2. So the light distribution $U(x,y)$ becomes

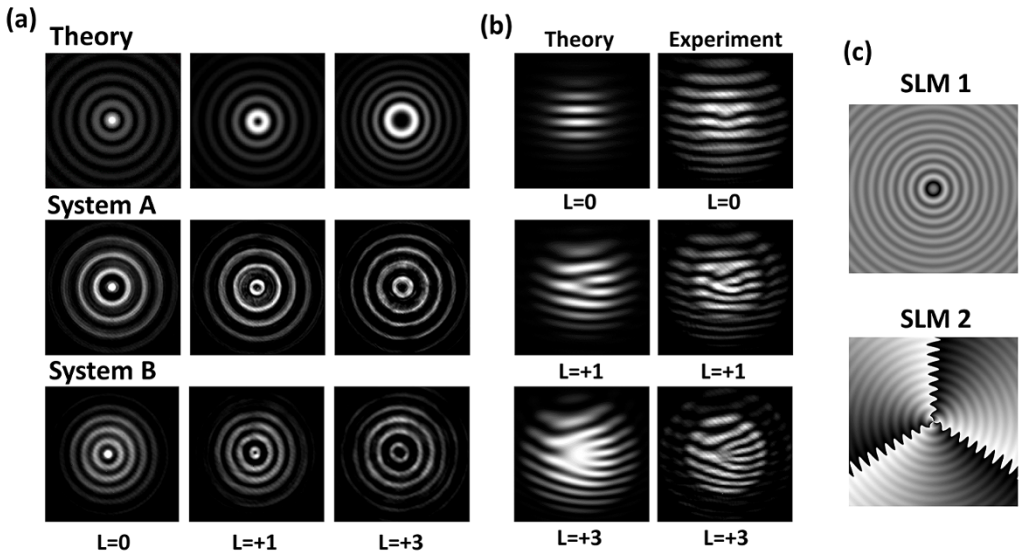

Figure 6 | (a) Theoretical and experimental results for the generation of Bessel beams ($l = 0, +1$ and $+3$). (b) Theoretical and experimental results of the interferograms when a Bessel beam and a Gaussian beam interfere with a small angle. (c) Phase patterns loaded onto SLM1 and SLM2 for generating Bessel beam with $l = +3$.

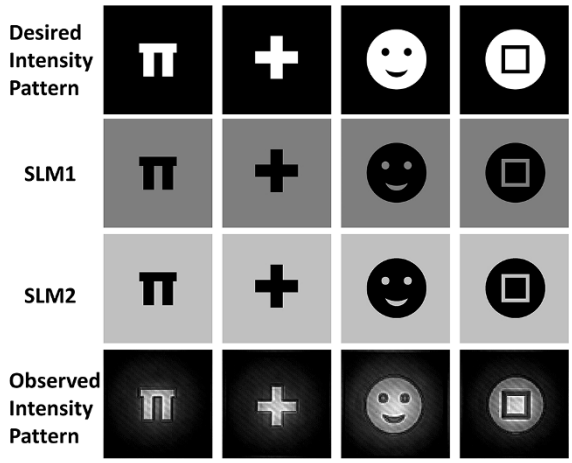

Figure 7 | Experimental results for the generation of arbitrary beams with odd-shaped intensity.

$$
\begin{aligned}
U(x,y) &= \frac{exp(jkf)\exp\left[j\frac{k}{2f}(x^2+y^2)\right]}{j\lambda f} \\
&\times \iint U_f(u,v)exp\left[j\frac{k}{2f}(u^2+v^2)\right]\exp\left[-j\frac{2\pi}{\lambda f}(xu+yv)\right]dudv \\
&= \frac{exp(jkf)\exp\left[j\frac{k}{2f}(x^2+y^2)\right]}{-\lambda^2 f^2} \\
&\times \iint\iint A(\xi,\eta)\exp\left[-j\frac{2\pi}{\lambda f}(\xi u+\eta v)\right]d\xi d\eta\exp\left[-j\frac{2\pi}{\lambda f}(xu+yv)\right]dudv \\
&= \frac{exp(jkf)}{-\lambda^2 f^2}\exp\left[j\frac{k}{2f}(x^2+y^2)\right]A(-x,-y)
\end{aligned}
\tag{4}
$$

From Eq. (4), it is found that the one-lens imaging system images the plane of SLM1 to that of SLM2 with unit magnification (inverted image), i.e. such imaging system can retrieve both amplitude and phase information of SLM1 plane at the position of SLM2 plane. Moreover, it is noted that an additional radial phase distribution $\exp\left(i\frac{k}{2f}(x^2+y^2)\right)$ is introduced as a separable term in the image at the SLM2 plane. Such radial phase distribution does not impact the successful generation of desired beam with both amplitude and phase manipulation, while might influence the propagation property of the generated beam. Remarkably, one can remove such radial phase distribution by updating the phase pattern loaded onto the SLM2, i.e. adding an extra inverted radial phase distribution to SLM2.

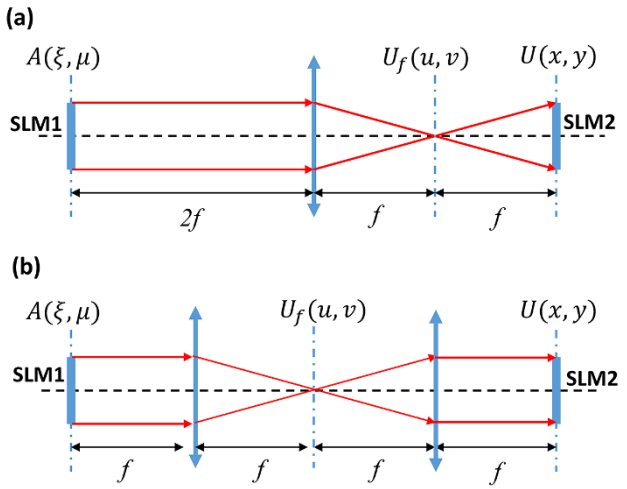

Figure 8 | Imaging illustration of (a) System A and (b) System B.

Another option to remove the unwanted radial phase distribution in System A is to employ a well-known 4f system. As depicted in Fig. 8(b), for the 4f system (System B), we can also use theories in Fourier optics to analyze the imaging characteristics. The two lenses in the 4f system both perform the Fourier transform. Firstly, the light comes through the first lens and is focused by the lens. It is an exact Fourier transform relationship between the SLM1 plane and the focal plane of the first lens. So the light distribution $U_f(u, v)$ at the focal plane of the first lens can be expressed by

$$
U_f(u,v) = \iint A(\xi,\eta)\exp\left[-j\frac{2\pi}{\lambda f}(\xi u+\eta v)\right]d\xi d\eta \tag{5}
$$

Then the light passes through the second lens which performs another Fourier transform. It is also an exact Fourier transform relationship between the focal plane of the first lens and the focal plane of the second lens. So the light distribution $U(x, y)$ at the focal plane of the second lens can be written by

$$
U(x,y) = \iint U_f(u,v)\exp\left[-j\frac{2\pi}{\lambda f}(xu+yv)\right]dudv \tag{6}
$$

Substituting Eq. (5) into (6), we can get

$$
\begin{aligned}
U(x,y) &= \iint\iint A(\xi,\eta)\exp\left[-j\frac{2\pi}{\lambda f}(\xi u+\eta v)\right]d\xi d\eta\exp\left[-j\frac{2\pi}{\lambda f}(xu+yv)\right]dudv \\
&= A(-x,-y)
\end{aligned}
\tag{7}
$$

From Eq. (7), one can clearly see that the 4f system also images the plane of SLM1 to that of SLM2 with unit magnification (inverted image). In particular, no additional radial phase distribution as in System A is introduced in System B. Hence, almost perfect imaging from the SLM1 plane to the SLM2 plane is achievable.

Remarkably, one may still observe some distortions in the experimental results compared to theories. Such phenomena might be further explained as follows.

1) The incident light to the SLM1 is actually not perfect plane wave, which is different from the assumption.
2) In practical configurations of System A (one-lens imaging system) and System B (4f system), the distance between the two SLMs might not be exactly the same as designed, which could induce unwanted phase distribution.
3) The lenses in the configurations might not be placed at precise positions as expected causing possible deviation of phase distribution.
4) Slight deviation from perfect light path alignment (e.g. offset from the center of SLMs and lenses) might introduce unwanted aberration.
5) The lenses used in the experiment might have slight deviation from desired perfect curvature.
6) The SLMs employed in the experiment might suffer slight imperfect phase modulation calibration (e.g. over/under phase modulation of 2π), nonideal phase modulation characteristics (e.g. nonlinear phase response), and deviation from perfect flatness (e.g. surface curvature).
7) The non-unity efficiency of SLMs cause non-pure contribution from the zero-order non-diffracted light, which might degrade the purity of the generated beams.

With future improvement, the performance degradation due to those possible imperfections of incident light beam, light path alignment, phase and flatness calibration might be compensated by carefully designing the phase patterns loaded onto SLM1 and SLM2. For

the performance degradation due to non-unity efficiency, SLMs with higher light utilization efficiency are preferred to improve the purity of generated beams. Using SLMs in the diffractive mode to remove the non-pure contribution from the zero-order light could be an alternative way to effectively improve the purity of generated beams. In order to fully characterize the purity of the generated different kinds of beams with both amplitude and phase modulation, accurate measurements of generated beams would be considered using wavefront sensors. Additionally, adaptive optics could be also considered to compensate the aforementioned imperfections and further effectively improve the operation performance.

Method

Devices in the experimental setup. The two SLMs we used in the experiments are both Holoeye PLUTO phase-only SLMs based on reflective LCOS microdisplays. These SLMs have a spatial resolution of 1920 × 1080 pixels and a pixel size of 8 μm. The illumination angle of the SLMs is about 7.2°. The resolution of the phase patterns prepared and displayed on the SLMs is 1080 × 1080 pixels (square shape). The phase patterns are set at the center of the SLMs. The camera used in the experiment is a HAMAMATSU InGaAs camera.

Phase pattern generation. Here, we take the generation of multiple collinear OAM beams as an example to illustrate the method. For multiple collinear OAM beams with topological charges $\{l_1, l_2, \ldots, l_n\}$, normally the electrical field can be described as follows

$$\begin{aligned} E(x,y) &= A_0[\exp(il_1\varphi(x,y)) + \cdots + \exp(il_n\varphi(x,y))] \\ &= A_0 B(x,y)\exp(i\Phi(x,y)) \end{aligned} \tag{8}$$

where A_0 is the amplitude of each OAM beam, $B(x, y)$ is the normalized amplitude distribution, and $\Phi(x, y)$ is the phase distribution. From Eq. (8), one can clearly see that the electrical field of multiple collinear OAM beams is a complex form, including both phase and amplitude distributions. Because of the spatially-variant amplitude distribution $B(x, y)$, the target multiple collinear OAM beams, in principle, cannot be realized by the traditional method using a single phase-only element.

By comparing Eq. (8) with Eq. (2), we can calculate following desired phase patterns

$$\varphi_1(x,y) = 2\arccos(B(x,y)) \tag{9}$$

$$\varphi_2(x,y) = \Phi(x,y) - \frac{1}{2}\varphi_1(x,y) \tag{10}$$

Thus, we can load $\varphi_1(x, y)$ and $\varphi_2(x, y)$ onto SLM1 and SLM2 to generate multiple collinear OAM beams.

For generating LG beams and Bessel beams, similar methods can be used to calculate the required phase patterns $\varphi_1(x, y)$ and $\varphi_2(x, y)$. We can write these patterns onto the corresponding SLMs to generate different beams. As a consequence, we can use two phase-only SLMs to realize arbitrary full field control (i.e. amplitude and phase manipulation) of a light beam. It could be a convenient and flexible way to arbitrarily generate different kinds of light beam with specific properties.

1. Márquez, A. *et al.* Programmable apodizer to compensate chromatic aberrations effects using a liquid crystal spatial light modulator. *Opt. Express* **13**, 716–730 (2005).
2. Osten, W. *et al.* Evaluation and application of spatial light modulators for optical metrology. *Opt. Pura Apl.* **38**, 71–81 (2005).
3. Dou, R. *et al.* Closed-loop adaptive optics system with a liquid crystal television as a phase retarder. *Opt. Lett.* **20**, 1583–1585 (1995).
4. Weiner, A. M. Femtosecond pulse shaping using spatial light modulators. *Rev. Sci. Instr.* **71**, 1929–1960 (2000).
5. Gopinathan, U. *et al.* A projection system for real world three dimensional objects using spatial light modulators. *J. Dispplay Technol.* **4**, 254–261 (2008).
6. Grier, D. G. A revolution in optical manipulation. *Nature* **424**, 810–816 (2003).
7. Karim, M. A. *et al.* Electrooptic display for optical information processing. *Proc. IEEE* **84**, 814–827 (1996).
8. Yu, W. *et al.* Polarization-multiplexed diffractive optical elements fabricated by subwavelength structures. *Appl. Opt.* **41**, 96–100 (2002).
9. Moreno, I. *et al.* Complete polarization control of light from a liquid crystal spatial light modulator. *Opt. Express* **20**, 364–376 (2012).
10. Chen, H. *et al.* Generation of vector beam with space-variant distribution of both polarization and phase. *Opt. Lett.* **36**, 3179–3181 (2011).
11. Rong, Z. Y., *et al.* Generation of arbitrary vector beams with cascaded liquid crystal spatial light modulators. *Opt. Express* **22**, 1636–1644 (2014).
12. Wang, J. *et al.* Terabit free-space data transmission employing orbital angular momentum multiplexing. *Nat. Photon.* **6**, 488–496 (2012).
13. Bozinovic, N. *et al.* Terabit-scale orbital angular momentum mode division multiplexing in fibers. *Science* **340**, 1545–1548 (2013).
14. Yan, Y. *et al.* Multicasting in a spatial division multiplexing system based on optical orbital angular momentum. *Opt. Lett.* **38**, 3930–3933 (2013).
15. Allen, L. *et al.* Orbital angular momentum of light and the transformation of Laguerre-Gaussian laser modes. *Phys. Rev. A* **45**, 8185–8189 (1992).
16. Yao, A. M. *et al.* Orbital angular momentum: origins, behavior and applications. *Adv. Opt. Photon.* **3**, 161–204 (2011).
17. Franke-Arnold, S. *et al.* Advances in optical angular momentum. *Laser Photon. Rev.* **2**, 299–313 (2008).
18. Gibson, G. *et al.* Free-space information transfer using light beams carrying orbital angular momentum. *Opt. Express* **12**, 5448–5456 (2004).
19. Kirk, J. P. *et al.* Phase-only complex-valued spatial filter. *JOSA* **61**, 1023–1028 (1971).
20. Leach, J. *et al.* Vortex knots in light. *New J. Phys.* **7**, 55 (2005).
21. Makowski, M. *et al.* Complex light modulation for lensless image projection. *Chin. Opt. Lett.* **9**, 120008 (2011).
22. Bolduc, E. *et al.* Exact solution to simultaneous intensity and phase encryption with a single phase-only hologram. *Opt. Lett.* **38**, 3546–3549 (2013).
23. Jesacher, A. *et al.* Near-perfect hologram reconstruction with a spatial light modulator. *Opt. Express* **16**, 2597–2603 (2008).
24. Jesacher, A. *et al.* Full phase and amplitude control of holographic optical tweezers with high efficiency. *Opt. Express* **16**, 4479–4486 (2008).
25. Siemion, A. *et al.* Diffuserless holographic projection working on twin spatial light modulators. *Opt. Lett.* **37**, 5064–5066 (2012).
26. Gerchberg, R. W. *et al.* A practical algorithm for the determination of phase from image and diffraction plane pictures. *Optik* **35**, 237–246 (1972).
27. Durnin, J. *et al.* Diffraction-free beams. *Phys. Rev. Lett.* **58**, 1499–1501 (1987).
28. Turunen, J. *et al.* Holographic generation of diffraction-free beams. *Appl. Opt.* **27**, 3959–3962 (1988).
29. Vasara, A. *et al.* Realization of general nondiffracting beams with computer-generated holograms. *J. Opt. Soc. Am. A* **6**, 1748–1754 (1989).
30. Indebetouw, G. Nondiffracting optical fields: some remarks on their analysis and synthesis. *J. Opt. Soc. Am. A* **6**, 150–152 (1989).
31. Bouchal, Z. *et al.* Self-reconstruction of a distorted nondiffracting beam. *Opt. Commun.* **151**, 207–211 (1998).
32. Litvin, I. *et al.* A conical wave approach to calculating Bessel-Gauss beam reconstruction after complex obstacles. *Opt. Commun.* **282**, 1078–1082 (2009).
33. Goodman, J. W. *Introduction to Fourier optics* [102–106] (McGraw-Hill, New York, 2005).

Acknowledgments

This work was supported by the National Basic Research Program of China (973 Program) under grant 2014CB340004, the National Natural Science Foundation of China (NSFC) under grants 11274131, 61222502 and L1222026, the Program for New Century Excellent Talents in University (NCET-11-0182), the Wuhan Science and Technology Plan Project under grant 2014070404010201, the Fundamental Research Funds for the Central Universities (HUST) under grants 2012YQ008 and 2013ZZGH003, and the seed project of Wuhan National Laboratory for Optoelectronics (WNLO). The authors thank Shuhui Li and Jun Liu for helpful discussions.

Author contributions

J.W. developed the concept and conceived the experiments. L.Z. carried out the experiments. L.Z. and J.W. analyzed the experimental data. L.Z. and J.W. contributed to writing and finalizing the paper.

Additional information

Competing financial interests: The authors declare no competing financial interests.

How to cite this article: Zhu, L. & Wang, J. Arbitrary manipulation of spatial amplitude and phase using phase-only spatial light modulators. *Sci. Rep.* **4**, 7441; DOI:10.1038/srep07441 (2014).